Dear Editor:

Thank you very much for your email dated August 21, 2025, which reminded us of one referee's report for our submitted manuscript on the SciPost Website.

In general, the referee 1 (Dr. Hu) gave a relatively positive evaluation of our work and stated that "basically this work can be accepted by Scipost." We appreciate his positive comment. In addition, the referee also proposed some comments/suggestions and hoped that we could add some more discussions and make minor revision. In response to the report, we have attached a point-to-point response below. We will make corresponding revisions of our manuscript after the recommendation from the Editor-in-charge.

Thank you very much for your assistance.

Yours sincerely
Yu-Chen Zhuang and Qing-Feng Sun

==========

Response to Report # 1 by Jin-Xin Hu (Referee 1)

==========

We are very grateful for Dr. Hu of reviewing our work and giving a valuable report. Below we present our reply to the referee's comments and suggestions. The corresponding revisions of our manuscript will await after the recommendation from the Editor-in-charge.

Comment:
Basically this work can be accepted by Scipost.

Reply: We thank the referee for the positive comments on our manuscript.

Comment:
But I suggest the authors to seriously consider adding more discussions about the trigonal warping effect, or some simulations. In my opinion, the current induced three pockets switching is important for the SDE observed in twisted trilayer graphene (Lin. et al).

Reply: We thank the referee for the helpful suggestion.

Trigonal warping is a fundamental effect of the energy bands for graphene and twisted multilayer graphene systems. It means that the originally rotationally symmetrical Fermi contour (isoenergetical line) is deformed into a shape like the triangle/triangle star, reflecting C_{3z} symmetry of the system. The emergence of trigonal warping effect can be related to multiple factors, such as the energy position and interlayer next-nearest-neighbor couplings. In some special cases, the trigonally warped closed Fermi surface may be further broken into three disconnected pockets (as suggested by the referee), which corresponds to a so-called Lifshitz transformation. The relevant physics and correlated phases mediated by the trigonal warping effects have been investigated and experimentally reported in bilayer graphene [Nature **608**, 298 (2022)], rhomobohedral trilayer graphene [Nature **598**, 429 (2021)], twisted bilayer graphene [Science **372**, 264 (2021)], twisted trilayer graphene [Nat. Mater. **23**, 356 (2024), Nat. Mater. **21**, 877 (2022)], etc.

In terms of our work, the key effect of trigonal warping lies in the breaking of the intravalley inversion symmetry within each valley band: $\epsilon_\tau(\mathbf{k}) \neq \epsilon_\tau(-\mathbf{k})$. In the manuscript, we used an 1D model with direct hypothesis of intravalley inversion symmetry breaking to illustrate the appearance of extreme nonreciprocal SDE. In fact, we also mention that one possible origin of this symmetry breaking in realistic twisted multilayer graphene bands is trigonal warping effect. Especially, the broken intravalley inversion symmetry is quite significant for current-induced valley polarization modulations and (extreme nonreciprocal) SDE in valley-polarized systems. On the one hand, when applying an electric current, the variation of electron occupations for left movers and right movers cannot be offset due to the **unequal Fermi velocities** of asymmetrical energy

bands [see Fig. 1(a) of our manuscript]. Then, the total electron occupation on each valley and valley polarizations can be modulated by applied currents. On the other hand, the combination of the valley polarization and intravalley inversion symmetry breaking makes **the intervalley Cooper pairings favor a finite momentum** (i.e., Fulde-Ferrell states), which leads to the emergence of SDE [see Figs. 2(d,e) in our manuscript].

To explicitly manifest the symmetry breaking brought by the trigonal warping effect, **we simply take a low-energy effective 2D continuum band $E^{eff}_{k_x,k_y,\tau}$ of the magic-angle twisted bilayer graphene as an example for detailed discussions** [Phys. Rev. Res. **5**, 023029 (2023), Phys. Rev. Lett. **130**, 266003 (2023)]. The discussion is basically similar for other twisted multilayer graphene systems. The valley bands can be written as:

$$E^{eff}_{k_x,k_y,\tau} = \epsilon^{eff}_{k_x,k_y,\tau} - \tau h_v - \tilde{\mu} = \lambda_0(k_x^2 + k_y^2) + \tau\lambda_1 k_x(k_x^2 - 3k_y^2) - \tau h_v - \tilde{\mu} \tag{R1}$$

where the index $\tau = \pm$ denotes K/K' valley. The parameter λ_0 and λ_1 denotes the kinetic coefficient and trigonal warping coefficient, respectively. Similar to the mean-field 1D band in Sec. 2.1 in our manuscript, h_v and $\tilde{\mu}$ here represent the interaction-induced valley splitting field and (modified) chemical potential. $\mathbf{k} = (k_x, k_y)$ is the wave vector relative to the Γ_m point in the moiré Brillouin zone. Actually, the effective low-energy band E^{eff}_{τ} can be also rewritten in polar coordinates: $E^{eff}_{k_r,\phi,\tau} = \lambda_0 k_r^2 + \lambda_1 k_r^3 \cos(3\phi)\tau_z - \tau h_v - \tilde{\mu}$ with the radial wave vector $k_r = \sqrt{k_x^2 + k_y^2}$ and the polar angle ϕ. We can see the term $\cos(3\phi)$ indicates a three fold symmetry.

In Figs. R1(a,b), we schematically demonstrate two typical types of Fermi contours of $E^{eff}_{k_x,k_y,\tau}$ close to Γ_m point with and without the trigonal warping effect. Compared to the isotropically circular Fermi contour ($\lambda_1 = 0$) [Fig. R1(a)], the trigonally warped Fermi contour has been deformed into a triangle-like shape with C_{3z} symmetry ($\lambda_1 \neq 0$) [Fig. R1(b)]. Additionally, we use red and blue colors to distinguish K band and K' band (plotted separately) in Fig. R1(b), and use distinct sizes of Fermi contours to imply a finite valley splitting. When applying an electric current j^x_{ext} in the bulk along the x direction, the Fermi level of right movers and left movers should be respectively lifted and declined by the electric voltage. Due to the asymmetry of trigonally warped Fermi contours, we can find the cases of Fermi velocities for right movers (purple arrows) and left movers (yellow arrows) are evidently different, which may also lead to a variation of the carrier occupation within one valley. For convenience, we can simply fix the quantum number k_y and regard the 2D effective model as an effective 1D model. Due to the symmetry breaking $E^{eff}_{k_x,\tau} \neq E^{eff}_{-k_x,\tau}$, the Fermi velocities along x direction for right movers $v^+_{F,\tau}$ and right movers $v^-_{F,\tau}$ is usually unequal, which is quite similar to Fig. 1(a) in our manuscript. In Fig. R1(c), we respectively show the 1D effective bands $E^{eff}_{\tau}(k_x)$ for $k_y = 0$ (left panel) and $k_y = 0.3$ nm^{-1} (right panel). They all exhibit asymmetrical feature, and band dispersions of left half and right half at the Fermi level (dark dashed lines) is different, corresponding to unequal Fermi velocities schematically denoted by colored arrows. It should also be noted that due to the time reversal relation between K band and K' band ($E^{eff}_{k_x,\tau} = E^{eff}_{-k_x,-\tau}$), the relative relationship between Fermi velocities of left movers and right movers is also opposite. For example, in Fig. R1(c), $v^+_{F,\tau} < v^-_{F,\tau}$ for $\tau = +$ (red band) while $v^+_{F,\tau} > v^-_{F,\tau}$ for $\tau = -$ (blue band). This

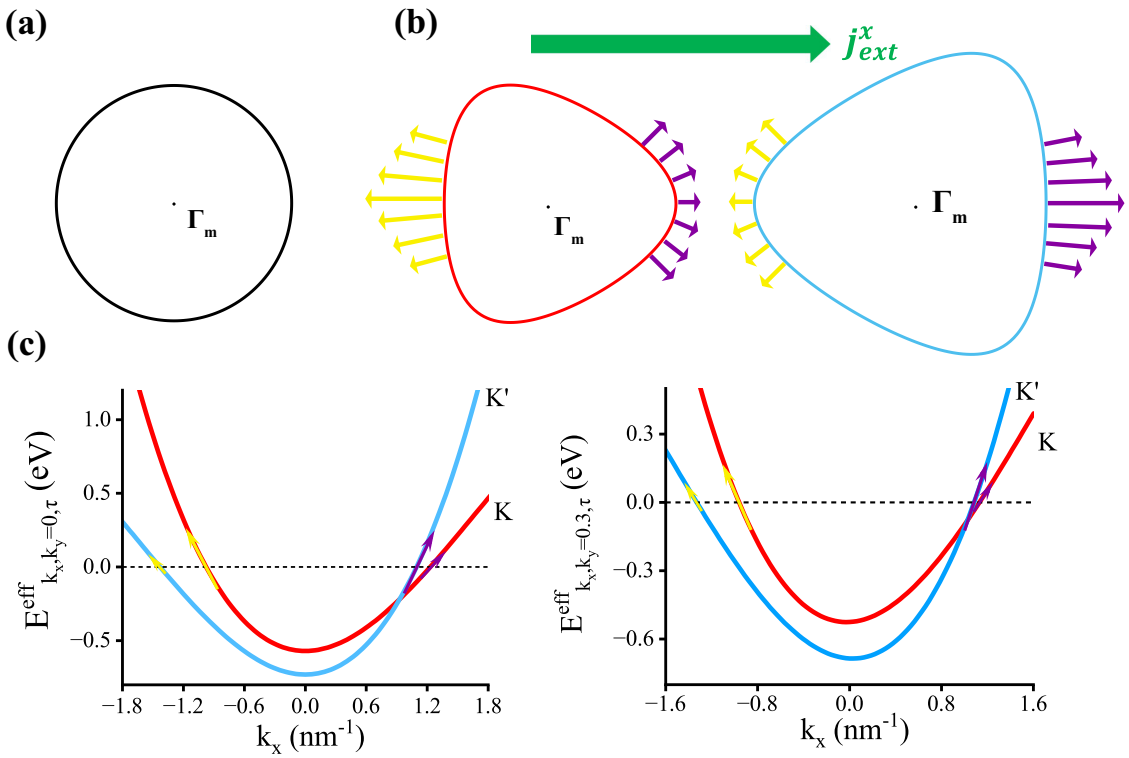

FIG. R1: (a) The schematic diagram for an isotropically circular Fermi contour of E^{eff}_{τ} around Γ_m point with $\lambda_1 = 0$. (b) The schematic diagram for typically trigonally warped Fermi contours around Γ_m point of E^{eff}_{τ} with $\lambda_1 \neq 0$. The red/blue color denotes K/K' valley, which are plotted separately for clarity. Purple arrows and yellow arrows schematically indicate local Fermi velocities of right and left movers, respectively. The electric current j^x_{ext} is applied along x direction. (c) the effective 1D valley bands $E^{eff}_{k_x,k_y,\tau}$ for the fixed $k_y = 0$ (left panel) and $k_y = 0.3$ nm^{-1} (right panel). The colored arrows also schematically indicate amplitudes of local Fermi velocities of effective 1D bands at the Fermi level (dark dashed lines). Here the model parameters (with units) are chosen as $\lambda_0 = 0.5$ eV nm^2, $\lambda_1 = -0.1$ eV nm^3, $\tilde{\mu} = 0.65$ eV, $h_v = -0.08$ eV.

guarantees the opposite modulation of electron occupations induced by the electric currents in two valley bands.

We can further generalize the formulas for current-induced valley polarization modulations in Appendix A from 1D model to 2D model. Considering an applied current j^x_{ext} along x direction with a bias V, they can be written as:

$$\begin{cases} n_\tau = \sum_{k_y,k_x} f[E^{eff}_{k_x,k_y,\tau} - \frac{eV}{2}\mathrm{sgn}(\frac{\partial E^{eff}_\tau}{\partial k_x})] \\ j^x_{ext} = \frac{e}{\hbar\mathcal{V}} \sum_{k_y,k_x,\tau} \frac{\partial E^{eff}_\tau}{\partial k_x} f[E^{eff}_{k_x,k_y,\tau} - \frac{eV}{2}\mathrm{sgn}(\frac{\partial E^{eff}_\tau}{\partial k_x})] \end{cases} \tag{R2}$$

Compared to formulas for 1D model, the formulas for 2D model additionally involves the summation over the quantum number k_y. Here $\mathcal{V}$ represents the size of the 2D system. Similarly, considering a small bias $V \to 0$, we can still derive a linear relation between n_τ,

h_v and j^x_{ext} (sheet current density), by using a Taylor expansion of eV:

$$\begin{cases} n_\tau \approx n^0_\tau + \alpha^x_\tau j^x_{ext} \\ h_v = \frac{U_v}{2\mathcal{V}}(n_+ - n_-) \approx \frac{U_v}{2\mathcal{V}}(\alpha^x_+ - \alpha^x_-) j^x_{ext} + h^0_v \end{cases} \tag{R3}$$

The n^0_τ and h^0_v denote the initial electron number and valley spitting without the applied current, respectively. The coefficient α^x_τ can be arranged as:

$$\alpha^x_\tau = \frac{\mathcal{V}\hbar}{e} \frac{\sum_{k_x,k_y} f'(E^{eff}_{k_x,k_y,\tau}) \mathrm{sgn}(\frac{\partial E^{eff}_\tau}{\partial k_x})}{\sum_{k_x,k_y,\tau} \frac{\partial E^{eff}_\tau}{\partial k_x} f'(E^{eff}_{k_x,k_y,\tau}) \mathrm{sgn}(\frac{\partial E^{eff}_\tau}{\partial k_x})} \tag{R4}$$

For the zero temperature limit and small bias, we can simply approximate the modulation of electron occupation Δn_τ for valley τ as:

$$\Delta n_\tau = n_\tau - n^0_\tau \approx \frac{\mathcal{V}}{(2\pi)^2} \frac{eV}{2} \times \left(\int_{l_1} \frac{dl}{|\nabla_{\mathbf{k}} E|} - \int_{l_2} \frac{dl}{|\nabla_{\mathbf{k}} E|} \right) \tag{R5}$$

Here l_1 and l_2 represent the part of Fermi contour for right movers (purple arrows) and left movers (yellow arrows), respectively. $|\nabla_{\mathbf{k}} E|$ is related to the magnitude of local Fermi velocity. Since the trigonal warping breaks intravalley inversion symmetry, the subtraction between two integrals in Eq. (R5) is generally nonzero. A finite bias (electric current) can thus induce the modulation of electron occupation in one valley.

As stated before, the original closed Fermi contour in Fig. R1(b) could further break into three disconnected small Fermi pockets in some special cases. At this time, we agree with the referee that the populations among three pockets may be also changed by the current. **But focusing on the phenomenon of extreme nonreciprocal SDE, the valley polarization is regraded to play a leading role [Nat. Phys. 18, 1221 (2022)], which is only related to the summation of electron populations in three pockets.** Whether the Fermi contour is deformed into three pockets, the intravalley inversion symmetry has always been broken by trigonal warping effect, and the current-induced valley polarization modulation still exists.

Besides, in the superconducting phase, the simultaneous breaking of intravalley inversion symmetry and time reversal symmetry will induce Fulde-Ferrel states with finite momentum pairings. It breaks the equality of amplitudes of positive and negative depairing currents, as shown by the 1D model in Fig. 2(e) of our manuscript. The situation for 2D trigonally warped bands is in principle consistent, while the finite momentum pairing will now be three-fold degenerate. **Essentially, the interplay between current-induced valley polarizations and SDE still exists and the remodulation of depairing currents to actual critical currents possibly happens.** Therefore, the proposed mechanism of the extreme nonreciprocal SDE and current-induced re-entrant superconductivity remains valid.

In summary, the crucial effect of trigonal warping is the breaking of intravalley inversion symmetry of 2D valley bands. And our physical picture in the

manuscript can be generalized to 2D trigonally warped valley-polarized systems. We thank the referee again for the valuable comments. We plan to refine the above explanation and then supplement it along with Fig. (R1) as a new Appendix to discuss the trigonal warping effect in the revised manuscript. Some additional illustrations and references will be added in the new main text. The corresponding revisions of our manuscript will be made after the recommendation from the Editor-in-charge.